J. Mol. Biol. (1993) 234, 1230–1247

Crystal Structure of *Myxococcus xanthus* Nucleoside Diphosphate Kinase and its Interaction with a Nucleotide Substrate at 2·0 Å Resolution

Roger L. Williams[1,2]†, Deena A. Oren[2], José Muñoz-Dorado[3]‡, Sumiko Inouye[3] Masayori Inouye[3] and Edward Arnold[2]†

[1]*Centre for Protein Engineering*
Medical Research Council Centre
Hills Road, Cambridge, CB2 2QH, England

[2]*Center for Advanced Biotechnology and Medicine (CABM)*
and Rutgers University Chemistry Department
679 Hoes Lane, Piscataway, NJ 08854 5638, U.S.A.

[3]*Department of Biochemistry, Robert Wood Johnson Medical School*
University of Medicine and Dentistry of New Jersey
Piscataway, NJ 08854–5635, U.S.A.

(Received 29 June 1993; accepted 7 September 1993)

The X-ray crystallographic structure of nucleoside diphosphate (NDP) kinase from *Myxococcus xanthus* has been determined using multiple isomorphous replacement techniques and refined at 2·0 Å resolution to a crystallographic *R*-factor of 0·17. This is the first report of the structure of an enzymatically active NDP kinase and of the enzyme with a bound nucleotide. The structure has been determined in $P4_32_12$ and $I222$ crystal forms. The enzyme monomer consists of a four-stranded antiparallel β-sheet. The surfaces of the sheet are partially covered with five helical segments. There are two protein molecules in the asymmetric unit of the tetragonal crystal form. They form a dimer with an extensive interface in which 1092 Å^2 per monomer is buried. The majority of the contact area in the dimer interface is between hydrophobic or aromatic residues. Two dimers are related by a crystallographic 2-fold axis to yield a tetramer. This tetramer is also present in the orthorhombic crystals; however, in this case, the 222 symmetry is entirely crystallographic. Upon tetramer formation, an additional 473 Å^2 of solvent-accessible surface area from each monomer becomes buried. The interface between dimers in the tetramer is stabilized by salt bridges. Equilibrium sedimentation studies are consistent with the enzyme being a tetramer in solution.

The structure of a complex of adenosine diphosphate (ADP) with the enzyme was determined and reveals that most of the nucleotide interactions with the protein are with the pyrophosphate and ribose groups, while the base has no hydrogen bonds with the protein and interacts only by stacking with the side chain of Phe59. The Mg^{2+} interacts with the pyrophosphate of the ADP and *via* a solvent molecule with the side chain of the conserved Asp120 residue. The mode of interaction with the nucleotide is novel, with the nucleotide binding at the side of the β-sheet.

The structures of the nucleotide in crystals grown in the presence or absence of Mg^{2+} are essentially identical. In addition, the phosphotransfer reaction from adenosine triphosphate (ATP) to the enzyme can occur without Mg^{2+}. This suggests that only the second step of the reaction in which the enzyme transfers the phosphate to a nucleoside diphosphate acceptor is significantly catalyzed by the metal.

Keywords: phosphotransferase; nucleoside diphosphate kinase; nm23; protein crystallography; adenosine diphosphate binding

† Authors to whom all correspondence should be addressed.
‡ Present address: Central Research Laboratories of Key Technology, Kirin Brewery Co., Ltd., 13–15 Fukuura, Kanazawaku, Yokohama-shi, Kanagawa 236, Japan.

0022–2836/93/241230–18 $8.00/0

1. Introduction

Nucleoside diphosphate (NDP†) kinase (EC 2.7.4.6) catalyzes the transfer of the γ-phosphate from a nucleoside triphosphate (NTP) to a nucleoside diphosphate (NDP). NDP kinase is considered to be essential for the maintenance of pools of all NTP's and dNTP's in a cell, in both prokaryotic and eukaryotic organisms (Parks & Agarwal, 1973; Ginther & Ingraham, 1974). In *Myxococcus xanthus*, NDP kinase is essential for cell growth (Muñoz-Dorado *et al.*, 1990*a*). The pairwise homologies among enzymes from various species (including both prokaryotes and eukaryotes) range from 40% to 94% identity (Hama *et al.*, 1991).

In addition to the crucial role that NDP kinase plays in maintaining pools of nucleoside triphosphates, it has been implicated in developmental processes, oncogenic transformation and metastasis, microtubule assembly, and signal transduction *via* G proteins. The role of NDP kinase in oncogenic transformation is not completely defined. An increase in NDP kinase activity has been observed in malignant colon cells as compared with normal cells (Francis *et al.*, 1989). On the other hand, the NDP kinase gene *nm23* has been shown to be a suppressor of metastasis (Leone *et al.*, 1991).

In *Drosophila melanogaster*, mutations in the *prune* gene that has significant homology to Ras GTP-ase activating protein (GAP), affect the same pathway as a *Drosophila* NDP kinase gene, *awd* (Teng *et al.*, 1991). Heterozygous individuals with mutations in both *prune* and $awd^{K\text{-}pn}$ (*pn*; $awd^{K\text{-}pn}/awd^{+}$) die, whereas individuals with either mutation alone do not. The $awd^{K\text{-}pn}$ protein product itself has normal NDP kinase activity and is present in similar concentration to the wild type enzyme in larvae (Lascu *et al.*, 1992). It has been suggested that the proline to serine mutation in $awd^{K\text{-}pn}$ results in altered interactions between NDP kinase and other cellular proteins (Biggs *et al.*, 1990; Lascu *et al.*, 1992).

Direct interaction between NDP kinase and other cellular proteins such as G proteins and tubulin has been proposed (Nickerson & Wells, 1984; Ohtsuki *et al.*, 1986; Wieland & Jacobs, 1989; Kikkawa *et al.*, 1990; Liotta & Steeg, 1990). However, there appears to be no evidence for direct transphosphorylation of GDP bound to a G protein (Randazzo *et al.*, 1992). An alternative to the direct interaction is that NDP kinase simply alters the GTP/GDP ratio of nucleotide pools. Consistent with control of Ras-like proteins by GTP/GDP ratios is the recent observation that a mutation of a gene encoding guanylate kinase leads to neoplastic growth of imaginal disks in *D. melanogaster*, presumably due to decreased levels of GDP, the product of the guanylate kinase reaction (Woods & Bryant, 1991).

NDP kinase functions *via* a ping-pong mechanism in which a phosphoprotein intermediate is formed through a high-energy phosphate bond to a histidine residue (Mourad & Parks, 1966; Parks & Agarwal, 1973). The transfer of a phosphate from the enzyme to a nucleoside diphosphate is catalyzed by Mg^{2+}. However, for the *M. xanthus* NDP kinase, it has been shown that the formation of a phosphoenzyme intermediate can readily occur in the absence of divalent cations (Muñoz-Dorado *et al.*, 1990*b*). Both the formation of the intermediate and subsequent transfer to a nucleoside diphosphate can proceed much more rapidly in the absence of a divalent cation when the donor is the γ-sulfate analog of ATP, adenosine 5′-sulfatopyrophosphate ($ADPSO_3$) (Peliska & O'Leary, 1991).

NDP kinase has a very broad specificity for both the phosphate donor and acceptor. Both purine and pyrimidine ribo- and deoxyribonucleotides function as substrates of the enzyme. There is indication that 2′,3′-dideoxynucleotides are relatively poor substrates for the enzyme (Karlsson *et al.*, 1990).

Recent studies have indicated that the activity of the *M. xanthus* enzyme is accompanied by serine phosphorylation in addition to the histidine phosphorylation (Muñoz-Dorado *et al.*, 1993). Although roughly half of the phosphate linked to the enzyme after incubation with ATP is in the form of phosphoserine, it is not yet known whether this phosphorylation has any role in the mechanism or regulation of the enzyme.

Diffraction quality crystals have been reported for NDP kinase from *M. xanthus* (Williams *et al.*, 1991) and *D. discoideum* (Dumas *et al.*, 1991). The structure of an enzymatically inactive mutant of the *D. discoideum* NDP kinase was reported by Dumas *et al.* (1992). This report is the first description of the three-dimensional structure of an enzymatically active NDP kinase and of a complex of the enzyme with a nucleotide. This provides a foundation for understanding the structural aspects of the phosphate transfer reaction carried out by this enzyme.

2. Materials and Methods

(a) *Expression and purification of NDP kinase*

The initial protein used for crystallization was expressed in *Escherichia coli* JM83 cells harboring the PJM5C2A plasmid (Muñoz-Dorado *et al.*, 1990*a*,*b*). It was later found that DH5α cells (GIBCO-BRL) transformed with the same plasmid expressed greater quantities of NDP kinase. Due to an apparent instability in the number of copies of the plasmid, it was necessary to transform cells prior to each protein preparation. A single colony was inoculated in 0·5 l of LB medium with 100 μg/ml ampicillin. The liquid cultures (3 l) were grown to a density of A_{600} = 1·8 (12 to 15 h). Cells were harvested by centrifugation at 4000 *g* for 30 min, resuspended in 25 ml of TE buffer (10 mM Tris·HCl, pH 7·7, 1 mM EDTA) and disrupted by sonication. Cell debris was removed by

† Abbreviations used: NDP, nucleoside diphosphate; NTP, nucleoside triphosphate; ADP, adenosine diphosphate; ATP, adenosine triphosphate; GDP, guanosine diphosphate; GTP, guanosine triphosphate; MIR, multiple isomorphous replacement; IEF, isoelectric focusing; PEG, polyethylene glycol.

centrifugation at 4000 ***g*** for 15 min, followed by centrifugation at 100,000 ***g*** for 40 min. The supernatant was loaded on a 250 ml DEAE Sephacel (Pharmacia) column equilibrated in TE buffer. The NDP kinase eluted in the flow-through and was rechromatographed on a second, identical DEAE Sephacel column. The protein was concentrated to a volume of 12 ml, loaded on a 500 ml Sephadex G-100 column and eluted with TEN buffer (TE buffer with 0·1 M NaCl). The fractions containing NDP kinase were pooled, concentrated to 64 mg/ml (BioRad protein assay, with bovine serum albumin as a standard), and frozen. A typical preparation yields 100 mg of purified enzyme per liter of culture.

(b) *Crystallization and preparation of heavy-atom derivatives*

Three crystal forms were obtained. Forms I and II have *I*222 symmetry and were described previously (Williams *et al.*, 1991). Form III crystals (a = 63·5 Å, c = 158·0 Å, space group $P4_32_12$) were used for the initial structure determination. These crystals were obtained by vapor diffusion (McPherson, 1982). Equal volumes of the concentrated protein solution and a solution containing 0·3 M sodium acetate, 0·1 M acetic acid, 0·01 M EDTA and 13% polyethylene glycol (PEG) 3350 (final pH 5·2) were mixed and equilibrated against a reservoir containing the same solution except for 16% PEG 3350. Typical crystals had dimensions 0·3 mm × 0·3 mm × 0·5 mm. There are 2 molecules in the asymmetric unit of the form III crystals, whereas forms I and II have 5 and 1 molecules, respectively. Because the form III crystals have much lower mosaicity than the form II crystals and because they diffract to a limit of 1·7 Å, the structure determination focused on form III crystals.

Isomorphous derivatives of the native protein were prepared by soaking the crystals in various heavy-atom containing solutions. A wide survey of heavy-atom compounds yielded several that were useful for multiple isomorphous replacement (MIR) phasing. Most of these compounds gave derivatives with the same set of sites. Additional derivatives with unique sites were obtained by introducing cysteine residues using polymerase chain reaction (PCR) mutagenesis. Of the 5 cysteine mutants constructed, only 1 mutant, in which Ser25 was replaced by Cys (S25C), crystallized isomorphously to the wild-type protein. The remaining mutants crystallized in different space groups.

(c) *Data collection and reduction*

The MIR structure determination at 2·6 Å was based on data collected using a Xuong-Hamlin Mark II area detector (San Diego Multiwire Systems) mounted on a Rigaku RU-200 rotating anode generator with a graphite monochromator. Data were collected in 0·12° frames with exposure times from 25 to 45 s and were reduced with the Hamlin Multiwire software. The subsequent 2·0 Å structure determination was based on data collected with a MAR Research storage phosphor image plate scanner using either a rotating anode X-ray source (Enraf-Nonius GX-13) or a synchrotron radiation source (Station 9·5, λ = 0·92 Å, in Daresbury, U.K.). Complete data sets were obtained from single crystals. MAR Research scanner data were collected using a rotation angle of 0·25° or 0·3° per exposure. For the rotating anode X-ray source with the MAR Research scanner exposures were 10 min per image. Synchrotron data were collected using 30 s exposure per image. For both conventional and synchrotron data collection, the crystals were cooled to 0°C. The data were reduced using the program MADNES (Pflugrath, 1989) as modified for the MAR Research scanner (Evans, 1992).

The 2·0 Å refinement was based upon 20,979 reflections (all data between 6·0 Å and 2·0 Å resolution, 93·2% of possible reflections) obtained by merging data from two crystals (native data set B of Table 1).

(d) *Initial MIR structure determination for form III crystals*

The positions of the heavy atoms were determined from isomorphous difference Patterson maps using the program VECTORMAP (R.L.W. & E.A., unpublished results). The origins for various derivative data sets were correlated using cross difference Fourier analyses. The MIR phases were calculated and refined using the program PHASES (Furey, 1992). Automatic boundary determination, solvent averaging, and phase recombination were also carried out using PHASES. However, the final solvent averaged electron density map differed little from the non-averaged electron density map and both types of maps were used in the initial stages of model building. Protein phases resulting from solvent averaging were used in the heavy-atom refinement in an iterative process to improve initial estimates of the heavy-atom parameters (Rould *et al.*, 1989). This resulted in slight improvements in the overall figure of merit and in the electron density maps. The heavy-atom refinement was carried out in 2 stages: first using data to 3·0 Å, giving a figure of merit of 0·81, then with data to 2·6 Å yielding a final figure of merit of 0·70. Assuming space group $P4_12_12$, resulted in an electron density map that had left-handed helices. Upon recalculating the electron density with the enantiomorphic space group $P4_32_12$, the helices had the correct sense. The absolute configuration was confirmed using the anomalous dispersion data for *cis*-platin (Blundell & Johnson, 1976). The 2·6 Å MIR map calculated using the derivative data sets listed in Table 1, with the refined heavy-atom parameters summarized in Table 2, was readily interpretable and clearly indicated that there were 2 molecules in the asymmetric unit of the form III crystals. Models for each of the molecules in the asymmetric unit were independently built using the program O (Jones *et al.*, 1991). The model was refined with the 2·6 Å data using XPLOR (Brunger, 1992) and PROLSQ (Hendrickson & Konnert, 1980). The initial crystallographic R-factor was 0·51. The refinement was alternated with manual readjustment using $3|F_o|-2|F_c|$ difference maps. Subsequent to the initial refinement and rebuilding, the automatic refinement program (ARP) (Lamzin & Wilson, 1993) was used. ARP refinement converged at an R-factor of 0·19 for the 2·6 Å data. The model was manually readjusted using $2|F_o|-|F_c|$ amplitudes and the phases from ARP. The rebuilt model was then subjected to further refinement with PROLSQ and XPLOR. This structure was used as the initial model for refinement in the form II unit cell (see section (e)). The model for the form III unit cell was further refined based on the results of the form II unit cell refinement (see section (f)).

(e) *Structure determination for form II crystals*

Each of the 2 protein molecules from the asymmetric unit of the form III crystal was used separately to solve the structure of the form II crystals using molecular replacement. Whereas both molecules indicated the same

Table 1
Summary of diffraction data

Dataset	Resolution (Å)	Number of crystals	Number of unique reflections	R_{merge}[a]	Number of sites	Phasing power[c]
Native-A[d]	2·6	4	10,351	0·047		
Native-B[e]	2·0	2	21,862	0·097[b]		
ADP·Mg^{2+}/enzyme complex[f,g]	2·0	1	21,660	0·072[b]		
ADP/enzyme complex (no Mg^{2+})[g]	2·0	1	18,928	0·110[b]		
Wild-type derivatives[d]						
$K_2PtCl_2(NH3)_2$-1	3·0	1	5867	0·038	4	1·9
$K_2PtCl_2(NH3)_2$-2	2·6	1	11,693	0·069	4	3·0
$K_2PtCl_2(NH3)_2$-3	2·6	1	8935	0·116	4	1·8
$K_2PtCl_2(NH3)_2$-4	2·6	1	9162	0·064	4	2·5
$K_2PtCl_2(NH3)_2$-5	2·6	1	5082	0·067	4	2·5
HgUTP + $MgCl_2$	2·8	1	7075	0·055	4	1·1
HgUTP + EDTA	3·0	1	5593	0·060	4	1·0
K_2IrCl_6	2·6	1	8627	0·051	4	0·9
PCMBS	3·0	1	6163	0·063	2	0·5
S25C mutant derivatives[d]						
PCMBS-1	2·6	1	6837	0·079	3	0·7
PCMBS-2	2·6	1	5562	0·029	3	0·4
$AuCl_3KCl$	4·5	1	1527	0·075	5	0·8

The overall MIR figure of merit to 2·6 Å is 0·70.

[a,b] R_{merge} is the R-factor for merging all multiple observations from a single crystal when the data were collected from a single crystal or the R-factor for merging data from several crystals in the cases where data were collected from several crystals:

$$^{a}R_{merge} = \sum_h \sum_i ||F(h)_i| - |\bar{F}(h)|| / \sum_h |\bar{F}(h)|$$

where $F(h)_i$ is the i^{th} measurement for the structure factor amplitude of reflection h and $\bar{F}(h)$ is the mean structure factor amplitude for reflection h.

$$^{b}R_{merge} = \sum_h \sum_i |I(h)_i - \bar{I}(h)| / \sum_h \bar{I}(h)$$

where $I(h)_i$ is the i^{th} measurement for the intensity of reflection h, and $\bar{I}(h)$ is the mean intensity of this reflection.

[c] Mean value of heavy atom structure factor amplitude divided by residual lack of closure error.

[d] These datasets were used for the MIR structure determination; data were collected at Rutgers/CABM with an RU-200 X-ray source and San Diego Multiwire area detector.

[e] These datasets were used for the subsequent 2·0 Å refinement of the enzyme structure; one dataset was collected at the Daresbury synchrotron source (station 9.5, wavelength 0·92 Å) using a MAR Research image plate scanner and another dataset was collected at LMB MRC with a GX-13 X-ray source and a MAR Research image plate scanner.

[f] This dataset was used for the 2·0 Å refinement of the structure of the ADP/enzyme complex.

[g] Data were collected at LMB MRC with a GX-13 X-ray source and a MAR Research image plate scanner.

solution, the rotation and translation function peaks were much more significant relative to the general background for one of the molecules. This molecule was designated molecule R, while the other molecule in the asymmetric unit of the form III crystals was denoted molecule L. The rotation function was calculated using the program ALMN (Dodson, 1992). The translation function was calculated using the program TFSGEN (Dodson, 1992). The translation function peak was the highest in the translation function map (10 times the standard deviation of the map). The transformation relating molecule R to the form II unit cell based upon this rotation/translation solution was:

$$\mathbf{x}_{formII} = \mathbf{M}\mathbf{x}_{formIII} + \mathbf{t}$$

$$\mathbf{M} = \begin{bmatrix} -0.7110 & -0.0725 & -0.6994 \\ -0.7032 & 0.0716 & 0.7074 \\ -0.0012 & 0.9948 & -0.1019 \end{bmatrix}$$

$$\mathbf{t} = \begin{bmatrix} 40.65 \\ -12.15 \\ 3.75 \end{bmatrix}$$

This transformation implies that the axis that is the non-crystallographic 2-fold in the form III unit cell becomes the crystallographic 2-fold along the b axis in the form II unit cell. Using this transformation we obtained an initial model for the form II asymmetric unit. The crystallographic R-factor was initially 0·53. This initial model was refined at 2·6 Å using simulated annealing followed by Powell minimization with the program XPLOR. Subsequent to XPLOR refinement, the model was refined with PROLSQ bringing the R-factor to 0·17. Although the space group of the form II crystals could have been either $I222$ or $I2_12_12_1$ on the basis of diffraction symmetry alone, the success of the refinement assuming $I222$ indicated that the space group symmetry was actually $I222$. For the PROLSQ refinement, the weight placed on deviation from the observed amplitudes *versus* deviation from ideal geometry was varied cyclically. The model in the form II unit cell was not subjected to any manual rebuilding. The rms deviations from ideal distances were 0·03 Å, 0·087 Å, and 0·101 Å for bond lengths, 1–3 distances (bond angles), and planar 1–4 distances (planar dihedral angles), respectively.

Table 2

Refined heavy atom parameters

Compound	x	y	z	Occupancy[a]	Binding residue	Binding molecule
A. *Derivatives of wild-type enzyme*						
$K_2PtCl_2(NH3)_2$-1	−0·154	−0·505	−0·074	0·610	His117	L
	−0·462	−0·341	−0·081	0·816	His139	L
	−0·462	−0·638	−0·071	0·737	His139	R
	−0·772	−0·474	−0·094	0·876	His117	R
5-Hg-UTP	−0·159	−0·494	−0·075	0·246	His117	L
(+10 mM $MgCl_2$)	−0·470	−0·343	−0·084	0·212	His139	L
	−0·449	−0·633	−0·074	0·142	His139	R
	−0·768	−0·485	−0·094	0·198	His117	R
5-Hg-UTP	−0·492	−0·626	−0·074	0·254	His139	R
(+10 mM EDTA)	−0·439	−0·332	−0·077	0·588	His139	L
	−0·473	−0·645	−0·067	0·488	His139	R
	−0·473	−0·659	−0·079	0·126	His139	R
$K_2PtCl_2(NH3)_2$-2	−0·152	−0·503	−0·073	0·315	His117	L
	−0·463	−0·346	−0·080	0·322	His139	L
	−0·463	−0·631	−0·070	0·311	His139	R
	−0·773	−0·473	−0·094	0·409	His117	R
anomalous	−0·152	−0·504	−0·073	0·389	His117	L
	−0·462	−0·346	−0·080	0·439	His139	L
	−0·462	−0·630	−0·070	0·373	His139	R
	−0·773	−0·474	−0·094	0·545	His117	R
$K_2PtCl_2(NH3)_2$-3	−0·153	−0·504	−0·073	0·603	His117	L
	−0·464	−0·347	−0·080	0·617	His139	L
	−0·463	−0·631	−0·070	0·630	His117	R
	−0·773	−0·473	−0·093	0·788	His139	R
$K_2PtCl_2(NH3)_2$-4	−0·152	−0·504	−0·072	0·632	His117	L
	−0·464	−0·349	−0·080	0·678	His139	L
	−0·464	−0·631	−0·070	0·724	His139	R
	−0·773	−0·474	−0·093	0·840	His117	R
anomalous	−0·153	−0·510	−0·074	0·387	His117	L
	−0·463	−0·348	−0·078	0·434	His139	L
	−0·469	−0·631	−0·067	0·404	His139	R
	−0·773	−0·476	−0·092	0·537	His117	R
$K_2PtCl_2(NH3)_2$-5	−0·152	−0·504	−0·073	0·649	His117	L
	−0·464	−0·348	−0·080	0·718	His139	L
	−0·463	−0·631	−0·071	0·705	His139	R
	−0·774	−0·474	−0·093	0·859	His117	R
anomalous	−0·155	−0·502	−0·072	1·167	His117	L
	−0·464	−0·349	−0·079	1·286	His139	L
	−0·463	−0·628	−0·073	1·279	His139	R
	−0·772	−0·472	−0·094	1·486	His117	R
K_2IrCl_6	−0·124	−0·499	−0·082	0·108	His117	L
	−0·147	−0·497	−0·079	0·063	His117	L
	−0·794	−0·489	−0·098	0·142	His117	R
	−0·468	−0·036	−0·044	0·050	Glu80	L
PCMBS	−0·450	−0·337	−0·077	0·733	His139	L
	−0·793	−0·557	−0·105	0·476	His54	R
B. *Derivatives of S25C*						
$AuCl_3KCl$	−0·746	−0·137	−0·027	1·241	Cys25	L
	−0·849	−0·274	−0·004	0·281	Cys25	R
	−0·814	−0·201	−0·007	1·033	Cys25	R
	−0·786	−0·177	−0·018	1·246	Cys25	R
	−0·127	−0·853	−0·075	0·259	Lys17	L
PCMBS-1	−0·736	−0·108	−0·025	0·684	Cys25	L
	−0·818	−0·198	−0·007	0·386	Cys25	R
	−0·766	−0·176	−0·017	0·501	Cys25	R
PCMBS-2	−0·732	−0·109	−0·026	1·150	Cys25	L
	−0·816	−0·203	−0·006	1·236	Cys25	R
	−0·760	−0·180	−0·015	0·816	Cys25	R

Phasing was based upon isomorphous differences for all of the compounds and upon anomalous differences for 3 of the compounds. The parameters for the anomalous scatterers were refined independently. For the compounds in which anomalous differences were used, the refined parameters for the anomalous scatterers follow the parameters based upon isomorphous differences.

[a]Occupancy is in arbitrary units.

Table 3
Deviation of the final model from ideal geometry

	rms deviation	Target σ
Distances (Å)		
Bonds (1-2 neighbor)	0·021	0·020
Angles (1 3 neighbor)	0·052	0·040
Intraplanar (1-4 neighbor)	0·058	0·050
Planar groups (Å)	0·018	0·020
Chiral centers (Å^3)	0·135	0·120
Non-bonded contacts (Å)		
Single torsion	0·329	0·3
Multiple torsion	0·156	0·3
Possible hydrogen bond	0·263	0·3
Thermal factors (Å^2)		
Main-chain bond (1–2 neighbor)	1·31	1·5
Main-chain angle (1–3 neighbor)	2·06	2·0
Side-chain bond	2·60	2·5
Side-chain angle	3·96	
Torsion angles (°)		
Planar (e.g. peptide ω)	4·30	10
Staggered (e.g. aliphatic χ_1)	18·0	15
Orthonormal (e.g. aromatic χ_2)	30·8	45

The model consists of 2238 protein atoms and 157 water molecules. The rms deviation is with respect to the ideal geometry as defined by PROLSQ. The target σ's are those that were used for weighting geometric deviations from ideality in the final stages of structure refinement.

(f) *2·6 Å refinement of a symmetric form III unit cell*

Because the initial rotation and translation function solutions had not been as clear when using molecule L as the search image, we built a model for the asymmetric unit of the form III crystal using only the R molecule. This was done by deriving a rigid body transformation relating a set of α-carbons of R to those of L. For this purpose, we used a region of the molecule, residues 5 to 50, in which the rms deviations of the two molecules differed least after optimal superposition. This symmetric version of the unit cell was then refined at 2·6 Å using XPLOR simulated annealing and PROLSQ least squares refinement. Throughout this refinement, no symmetric constraints were imposed on the conformations of the 2 molecules in the asymmetric unit. The crystallographic *R*-factor converged at 0·21 with no manual readjustment. Because the *R*-factor was slightly better and the deviations from ideal geometry were slightly less for this model as compared to the initial model based on independently built molecules, it was used as the initial model for the 2·0 Å refinement.

(g) *2·0 Å structure refinement of form III crystals*

The 2·0 Å refinement was initiated with simulated annealing refinement and Powell minimization using XPLOR followed by refinement to convergence with PROLSQ. The model was then manually refitted to the $3|F_o|-2|F_c|$ difference electron density map. Following subsequent PROLSQ refinement, the crystallographic *R*-factor was 0·22. Based upon peaks in the $|F_o|-|F_c|$ difference electron density map with heights greater than 4 times the standard deviation of the map, 157 water molecules were added to the model. For both the protein atoms and water molecules, only temperature factors and positions were refined. Occupancies were fixed to unity. The hydrated model was refined to convergence with PROLSQ. The final *R*-factor was 0·17. The deviations of the bond angles and distances from ideality are illustrated in Table 3.

(h) *Substrate binding studies*

Co-crystals of the enzyme with ADP were grown using the same method as described for the native form III crystals except that drops contained additionally 4 mM ADP and 10 mM $MgCl_2$. To determine the position of the Mg^{2+} in the complex, data sets were also collected for crystals grown with ADP and without Mg^{2+}. Data were collected with the MAR Research scanner and a rotating anode X-ray source. The space group of the co-crystals was also $P4_32_12$ with a unit cell $a = 63·5$ Å, $c = 159·0$ Å, i.e. nearly identical to the native unit cell. The structure of the native enzyme was used to provide initial phases. The initial phases were refined using PROLSQ and a model consisting of only the protein atoms. An initial model of the substrate was built using electron density maps calculated with $|F_o|-|F_c|$ or $3|F_o|-2|F_c|$ amplitudes and phases from the refined protein model. The model of the protein/nucleotide complex was then refined using Powell minimization and simulated annealing with XPLOR. The final crystallographic *R*-factor for the 2·0 Å refinement of the enzyme/ADP complex was 0·229 with no solvent molecules incorporated into the model.

(i) *Equilibrium sedimentation*

In order to estimate the molecular mass of the enzyme in solution, the enzyme was first dialyzed against a solution of 0·2 M sodium acetate, 0·1 M acetic acid, 0·01 M EDTA (identical to the solution used to obtain form III crystals except that it contained no PEG). The protein was centrifuged at 15,000 rpm at 4°C in a Beckman LB-70 ultracentrifuge until radial scans through the cell indicated no change in the distribution of protein within the cell.

(j) *Autophosphorylation assay for enzyme activity*

The autophosphorylation of the enzyme was monitored as a shift in pI using non-denaturing, non-reducing isoelectric focusing polyacrylamide gels (IEF PAGE). To assay the phosphorylation of NDP kinase in solution, a reaction mixture containing 0·4 mM protein, 0·1 M buffer, 0·2 M sodium acetate and 10 mM EDTA was added to an equal volume of 2 mM nucleotide (ATP or ADP). The buffer consisted of either 0·1 M Tris·HCl (final pH 7·9) or 0·1 M acetate buffer (final pH 5·2). After 4 min, the mixture was diluted 3-fold with water and 1 μl of the mixture was loaded onto the gel. After focusing, gels were stained with Coomassie blue.

In order to verify that the shift to lower pI forms was not simply a consequence of binding the nucleotide, 2 controls were carried out: (1) ADP was used instead of ATP in the reaction mixture. (2) Assays were carried out with either [γ-^{32}P]ATP or [α-^{32}P]ATP.

For the assays with radiolabeled ATP, a solution containing 25 μM NDP kinase was reacted at pH 7·9 or pH 5·2 with either 10 μCi [γ-^{32}P]ATP (final concentration 83 nM) or [α-^{32}P]ATP (final concentration 166 nM). After 4 min incubation, 1 μl of the reaction mixture was loaded onto the IEF gel and electrophoresed. Following focusing, the gel was autoradiographed.

To demonstrate the autophosphorylation in NDP kinase crystals, single crystals (form III) were first incu-

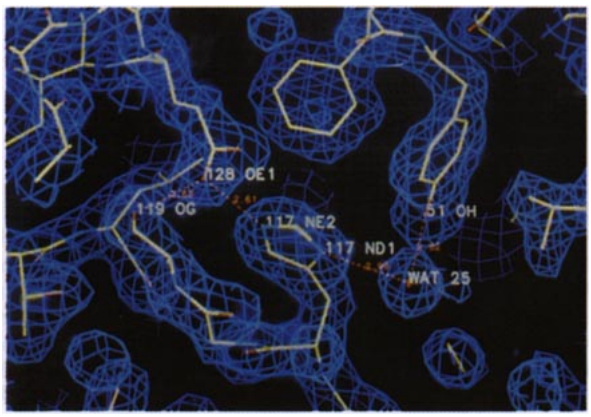

Figure 1. A view of a portion of the final $(2|F_{obs}|-|F_{calc}|)$ electron density map calculated using all data between 6·0 Å and 2·0 Å. The map is superimposed on the refined structure. The contour level is 1·2 times the standard deviation of the map. Shown is the pocket in the vicinity of the catalytic His117. There is an ordered solvent molecule labeled WAT 25 within hydrogen bonding distance of the catalytic histidine and the side-chain OH of Tyr51. This water molecule occupies a position nearly identical to the position of the 5′-terminal phosphate of a bound nucleotide. Glu128 forms possible hydrogen bonds with the catalytic histidine and with Ser119.

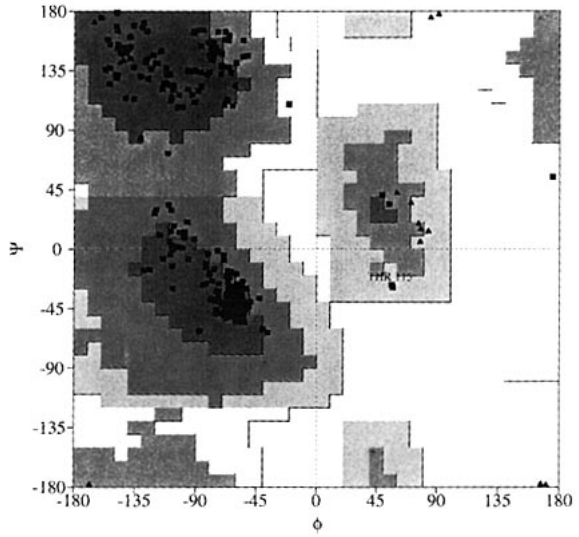

Figure 2. Ramachandran plot of the main-chain dihedral angles for all residues in the final refined model. The more preferred regions are indicated by darker filled areas. The disallowed regions are indicated by the lightest areas. Non-glycine residues are indicated by squares and glycine residues are indicated by triangles. The only non-glycine residues having ϕ angles greater than zero are Thr115 and the poorly ordered N-terminal alanine.

bated with the nucleotide for 15 h at 4·0°C in the pH 5·2 reaction mixture described above with 16% PEG 3350. Incubation was followed by extensive washing in a series of solutions in order to remove nucleotides. The crystals were then dissolved in 3 μl and a 1 μl portion was loaded onto an IEF gel.

3. Results and Discussion

(a) *MIR phasing*

The data used in the MIR phasing are summarized in Table 1. Most of the derivatives of the wild-type enzyme gave the same set of four sites (Table 2). These sites correspond to two histidine residues on each of the two molecules in the asymmetric unit; His117 that is phosphorylated in the enzymatic mechanism and His139. The S25C mutant provided an additional site that was essential for obtaining an unambiguous image of the protein in the electron density. In addition, the derivatives of the S25C mutant provided a "tag" that was useful for confirming that the sequence was in register with the electron density. The S25C mutant enzyme crystals were very sensitive to heavy atom-containing compounds. Extended times of soaking or concentrations greater than 1 mM resulted in extensive cracking of the crystals. Consequently, substitution for the S25C mutant crystals was generally less than that for the wild-type enzyme. In the structure, Ser25 is located in helix A1 (see below) very near the non-crystallographic 2-fold and is involved in the intermolecular contacts that stabilize the non-crystallographic dimer. However, it is not involved in intermolecular contacts elsewhere in the crystals. It is likely that this feature enabled the S25C mutant to crystallize isomorphously to the wild-type enzyme. The 5-Hg-UTP derivatives showed an interesting pattern of substitution. In the absence of Mg^{2+}, the reagent reacted only at His139 whereas in the presence of Mg^{2+}, substitution occurred at both His139 and the active site His117. The nucleotide 5-Hg-UTP can phosphorylate NDP kinase. It may be that in the presence of Mg^{2+}, this phosphoenzyme intermediate is destablized leaving His117 free for nucleophilic attack on the mercury. Without Mg^{2+}, the phosphoenzyme intermediate may be sufficiently stable that the His117 is not free to react with the mercury.

(b) *Model quality*

The electron density map calculated with $2|F_o|-|F_c|$ Fourier coefficients has density greater than the mean plus 1·2 standard deviations for all main-chain atoms except the N-terminal alanine and the C-terminal lysine (the N-terminal methionine encoded by the gene is not present in the protein expressed in *E. coli*). Figure 1 shows a representative region from the electron density map. A Ramachandran plot (Ramakrishnan & Ramachandran, 1965) for the main-chain dihedral angles is shown in Figure 2. All residues are within allowed regions of the Ramachandran plot. Except for Thr115 and the N-terminal alanine, all non-glycine residues have negative ϕ angles. Thr115 approximates a left-handed helical conformation.

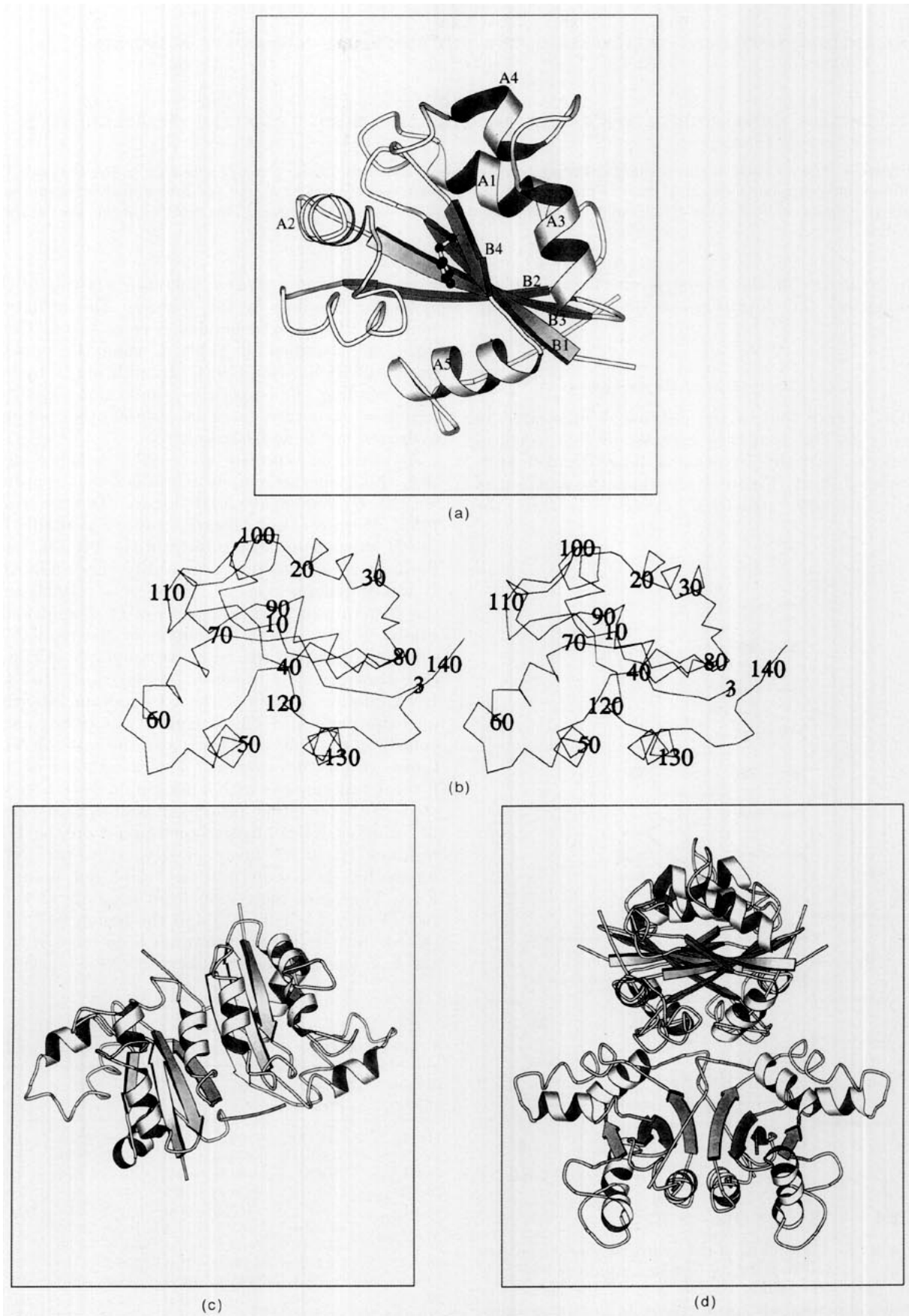

Figure 3. The overall fold of the NDP kinase as presented using the program MOLSCRIPT (Kraulis, 1991). (a) A ribbon schematic indicating the locations of the elements of secondary structure. (b) A stereo diagram of the C^{α} backbone. (c) A ribbon diagram of the non-crystallographically related dimer. (d) A ribbon representation of the tetramer with approximate 222 symmetry, generated by the operation of a crystallographic axis applied to the dimer.

```
1       10          20          30          40          50          60          70
MAIERTLSII KPDGLEKGVI GKIISRFEEK GLKPVAIRLQ HLSQAQAEGF YAVHKARPFF KDLVQFMISG
   |-B1--|          |---A1---|      |--B2--|                    |--A2---|

        80          90         100         110         120         130         140
PVVLMVLEGE NAVLANRDIM GATNPAQAAE GTIRKDFATS IDKNTVHGSD SLENAKIEIA YFFRETEIHS YPYQK
 |--B3--|   |--A3---|              |--A4-|        |B4|   |---A5-----|
```

Figure 4. The location of the elements of repetitive secondary structure in the primary sequence of the enzyme. The residue numbering begins at Met1 that is not present in the protein expressed in *E. coli* (as determined by amino acid analysis). Shown in bold is the HGSD motif that is present in all known NDP kinases. This motif contains the catalytic histidine.

The geometry of the model is excellent. Table 3 summarizes the deviations of the geometry from ideality.

(c) *Description of the monomer*

The overall fold of the enzyme is illustrated in Figure 3. The structure consists of five α-helical segments partially covering a four-stranded antiparallel β-sheet. Figure 4 identifies the location of the secondary structural elements within the sequence. Figure 5 gives a schematic drawing of the hydrogen bonding in the β-sheet. The structure contains 12 hydrogen-bonded reverse turns. These turns are classified in Table 4 using the nomenclature of Richardson (1981). In addition to hydrogen bonding in repetitive and non-repetitive secondary structure, there are several other possible hydrogen bonds and salt links.

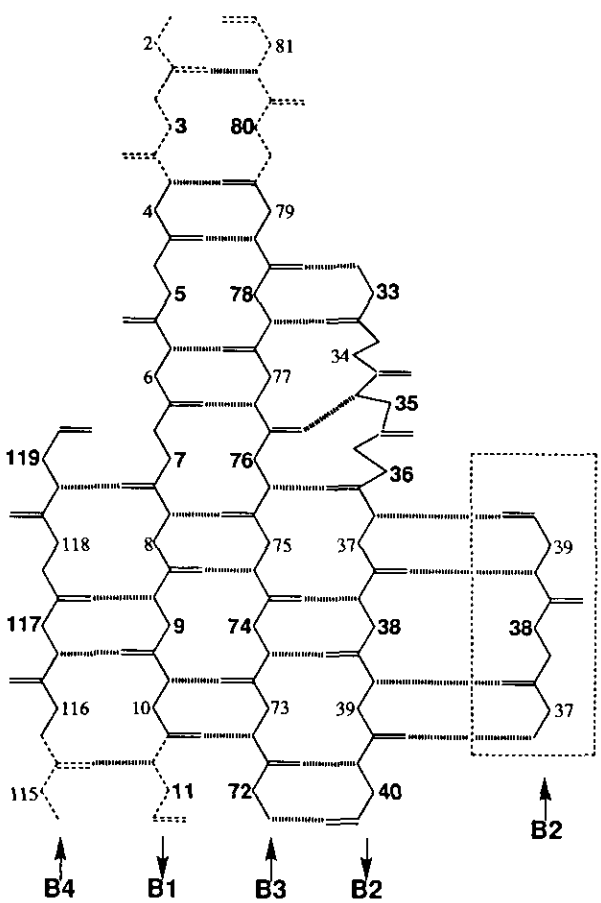

Figure 5. A schematic of the hydrogen bonding pattern in the 4-stranded β-sheet. Residues numbered in bold have their side chains on one side of the sheet. The residues numbered with plain type point toward the opposite side. The broken lines indicate residues forming main-chain hydrogen bonds at the edges of the β-sheet. The boxed residues are part of the non-crystallographically related β-sheet.

As would be expected, given 44% sequence identity, this structure closely resembles that reported for the *D. discoideum* NDP kinase (Dumas *et al.*, 1992). However, until coordinates are available for the *D. discoideum* structure from the Protein Data Bank, it is not possible to quantify this similarity. It was noted previously (Dumas *et al.*, 1992) that the structure of NDP kinase from *D. discoideum* is similar to the allosteric domain of the regulatory subunit of aspartate transcarbamylase (ATCase) (Kantrowitz & Lipscomb, 1988) and to the RNA-binding domain of the U1 small nuclear ribonucleoprotein A, U1A (Nagai *et al.*, 1990), particularly in the β-sheet. This is also the case for NDP kinase from *M. xanthus*. The α-carbons of the β-sheet superimpose with a maximum deviation less than 2·0 Å for either protein. Residues 2 to 122 of *M. xanthus* NDP kinase superimpose on the U1A residues 10 to 87 fairly closely. However, NDP kinase has two structural insertions not found in U1A. These are the region from residues 42 to 68 (which includes helix A2) and the region 90 to 115 (which includes a region that has been referred to as the Kpn loop). These structural insertions form two

Table 4

β-turns and their dihedral angles at positions 2 and 3

Residue numbers	Amino acid residues	ϕ_2 (°)	ψ_2 (°)	ϕ_3 (°)	ψ_3 (°)	Type
11–14	KPDG	−49·3	−39·9	−62·6	−31·1	III
15–18	LEKG	−55·8	−31·6	−80·8	−3·6	I
28–31	EEKG	−64·8	−29·2	−91·2	7·7	I
43–46	SQAQ	−58·4	−44·3	−57·2	−40·8	III
48–51	EGFY	−67·5	−40·3	−70·2	−41·4	III
52–55	AVHK	−63·8	−17·0	−106·4	17·5	I
54–57	HKAR	−64·7	−21·5	−82·3	−11·3	I
66–69	FMIS	−64·1	−17·5	−109·6	5·9	I
79–82	GENA	−71·4	132·4	48·9	40·9	IV
99–102	AEGT	−70·5	138·0	77·8	14·9	II
110–113	SIDK	−57·2	−40·7	−78·5	−37·9	III
135–138	ETEI	−73·6	−1·2	−102·8	1·2	I

In each case, there is an $i-i+3$ hydrogen bond. The classification is that described by Richardson (1981).

walls of the nucleotide-binding cleft in NDP kinase (see section (f) below).

(d) *Oligomeric structure of NDP kinase*

NDP kinase from various species has been reported to be trimeric, tetrameric, or hexameric. NDP kinase from *M. xanthus* was reported to be a trimer based on gel filtration chromatography (Muñoz-Dorado *et al.*, 1990*b*). We have carried out equilibrium sedimentation that yielded a molecular mass of 66 kDa, assuming a partial specific volume of 0·75 as calculated from the sequence using the method of Harpaz *et al.* (unpublished results). Given the 16 kDa mass of the NDP kinase, these data indicate that NDP kinase in solution is a tetramer. Apparently, the shape of the protein caused it to migrate anomalously in the previously reported gel filtration experiment. NDP kinases from rat mucosal mast cells and *Saccharomyces cerevisiae* have also been reported to be a tetramer (Jong & Ma, 1991; Hemmerich & Pecht, 1992). However, there are indications that NDP kinase from several sources is a hexamer. X-ray crystallographic structural analyses for NDP kinase from *D. discoideum* indicate that it is a hexamer (Dumas *et al.*, 1992). The *D. melanogaster* NDP kinase, Awd, is a hexamer based on gel filtration chromatography (Lascu *et al.*, 1992).

Our structural studies for both the form II and form III crystals are consistent with the observation that *M. xanthus* NDP kinase is a tetramer in solution. In the form III crystals there is a non-crystallographically related dimer. The 2-fold axis of this dimer is perpendicular to the crystallographic 2-fold at $z = 0$. This 2-fold interaction is also preserved in the form II crystals, and lies along the *b* axis. In the form III crystals, the angle between the non-crystallographic 2-fold axis and the *c* axis is about 97°, similar to the 90° between intersecting crystallographic 2-folds in the form II structure.

In general, the two molecules forming the non-crystallographically related dimer have similar conformations. The average rms deviation between C^{α} coordinates after optimal superposition (Kabsch, 1978) is 0·264 Å. The largest differences in conformation are in the region of residues 49 to 61 and the region 79 to 112 that includes what has been referred to as the Kpn loop (Dumas *et al.*, 1992) (Fig. 6A). These regions also have somewhat larger than average temperature factors (Fig. 6B) and greatest degree of solvent exposure in the tetramer (Fig. 6C, see below). This suggests that there may be some greater than average flexibility in these regions. The structure of the enzyme with bound substrate (see section (f) below) suggests that these regions change their conformations somewhat to accommodate substrate.

The contacts between the two molecules in the dimer are quite extensive (Fig. 7). The solvent-accessible surface area removed from each monomer upon formation of the dimer is 1092 Å^2 or 14% of the monomer solvent-accessible surface area (Lee &

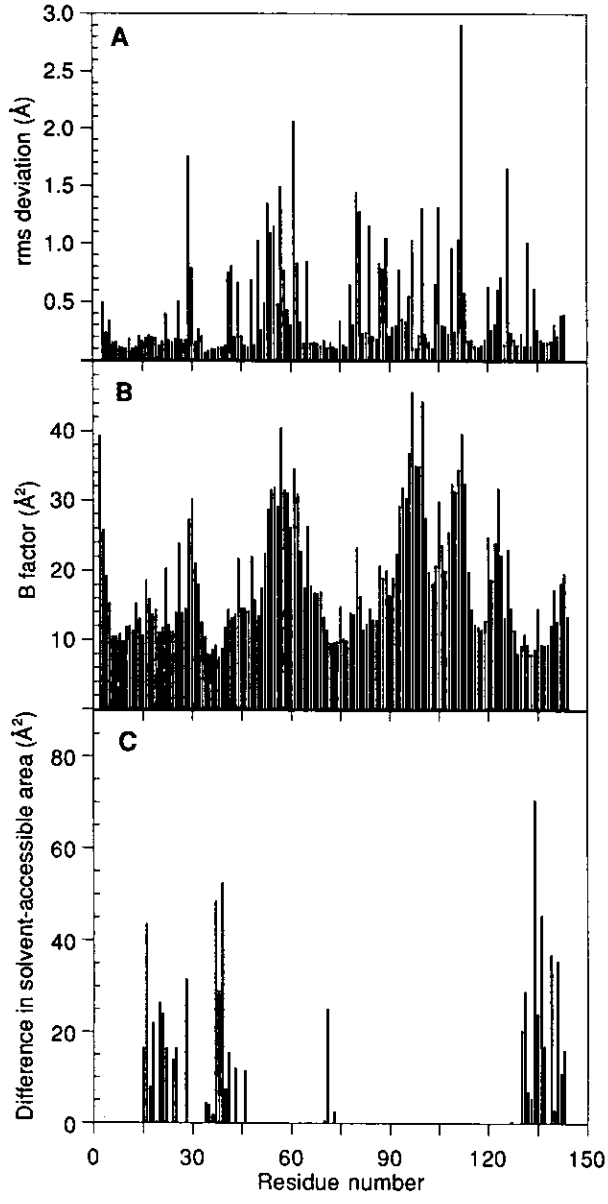

Figure 6. A. C^{α} rms deviation between the two molecules of the asymmetric unit after optimal rigid-body superimposition *versus* residue number. B. Average, isotropically refined temperature factor as a function of residue number. C. Average differences in solvent-accessible surface area between the monomer and the tetramer *versus* residue number.

Richards, 1971). For the calculations, a solvent sphere radius of 1·4 Å was assumed. The radii used for C, N, O, and S were 1·8 Å, 1·65 Å, 1·6 Å and 1·85 Å, respectively. The two molecules contact each other along the edges of their β-sheets. As indicated in Figure 5, the hydrogen-bonding pattern between molecules continues the antiparallel β-sheet hydrogen-bonding pattern found within each monomer. Hydrophobic or aromatic residues form most of the interface between the two molecules in the dimer. Of the 1092 Å^2 contact surface, 619 Å^2 are due to hydrophobic or aromatic residues. The dimer contacts are formed from residues in helical

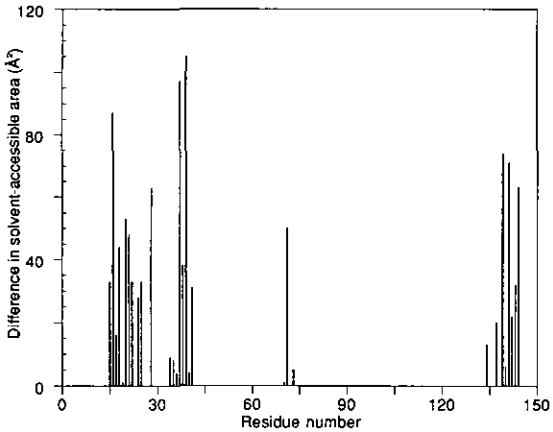

Figure 7. Average differences in solvent-accessible surface area between the monomer and the non-crystallographically related dimer *versus* residue number.

segment A1, the loop consisting of residues 12 to 17, β-strand B2, and the C-terminal region consisting of residues 134 to 144. The predominant pairwise interactions between structural elements (in decreasing order of buried surface) involve B2 and B2, A1 and A1, loop 12 to 17 and region 134 to 144, and B2 and region 134 to 144. The single residue with the largest change in solvent-accessible surface area (105 Å^2) upon association of the monomers to form the dimer is Leu39. The interactions between monomers in the non-crystallographic dimer are summarized in Table 5A.

The tetramer that is present in solution is probably identical to a tetramer in the form III crystals and arises from a crystallographic 2-fold axis perpendicular to and approximately intersecting the non-crystallographic 2-fold axis. In the tetramer, the molecules are arranged with their centers at vertices of a nearly regular tetrahedron so that the average center-to-center distance is 19 Å. A nearly identical tetramer is present in the form II crystal, however, the 222 symmetry in this case is exact. The additional solvent-accessible surface area removed from each monomer upon association of dimers to form a tetramer is 473 Å^2 or 6% of the monomer solvent-accessible surface area. In contrast to the dimer interface described above, only 17% of the solvent-accessible surface buried in the tetramer interface is due to aromatic or hydrophobic residues. The contacts between dimers are comprised of residues 36 to 45 and residues 129 to 142 (Fig. 6C). The residue with the largest surface area removed from accessibility to the solvent upon association of the monomers to form the tetramer is Arg134. The solvent-accessible surface area of Arg134 decreases from 165 Å^2 in the monomer to 24 Å^2 in the tetramer. This residue forms a possible salt bridge with a Glu137 from a dimer related by the crystallographic 2-fold. Because of the very limited solvent accessibility of the salt bridge in the tetramer, this interaction may be an important component of the stability of the tetramer. The interactions between two dimers in the tetramer are summarized in Table 5B.

Table 5

Protein-protein contacts within the tetramer

A. *Contacts within the dimer (between non-crystallographically related molecules R and L in the asymmetric unit)*

Possible hydrogen-bonding interactions		
Gly18-Glu28	Ile20-Glu28	Gly21-Glu28
Lys22-Ser25	Leu39-Ile37	Gln144-Glu16
Non-polar interactions		
Leu15-Tyr141	Leu15-Tyr143	Glu16-Pro142
Glu16-Gln144	Glu16-Tyr143	Gly18-Tyr143
Gly18-Glu28	Ile20-Glu28	Ile20-Tyr141
Gly21-Gly21	Gly21-Glu28	Gly21-Ile24
Ile24-Ile24	Pro34-Leu39	Val35-Leu39
Ile37-Arg38	Ile37-Leu39	Leu39-His139
His41-His139	Pro71-Tyr141	Pro71-His139

B. *Contacts between crystallographically related dimers in the tetramer. The interacting molecules are crystallographically related (y,x,−z) to molecules R and L in the asymmetric unit*

Possible hydrogen-bonding interactions or salt bridges		
Arg38-Arg134	Ala130-Glu135	Tyr131-Thr136
Phe132-Arg134	Arg134-Glu137	
Non-polar interactions		
Arg38-Arg134	Ser43-Ser43	Ala130-Arg134
Tyr131-Arg134	Tyr131-Glu135	Phe133-Arg134
Arg134-Arg134		

For possible hydrogen bonds, all contacts shorter than 3·5 Å with Donor–H···Acceptor bond angle greater than 120° and X–O···H bond angle greater than 90° are shown. For possible salt bridges, contacts shorter than 3·5 Å are listed. Non-polar interactions closer than 4·0 Å are listed. Interactions were classified as non-polar if they involved atoms other than O or N.

(e) *Enzymatic activity of the crystals*

Addition of nucleoside triphosphates to the crystals resulted in a multiplet of lower pI forms of the enzyme (Fig. 8). This shift in pI was due to transfer of the γ-phosphate of ATP to the protein (Fig. 8C). Formation of the phosphoprotein intermediate is similar at pH 5·2 (the pH at which form III crystals were obtained) and pH 7·9. The autophosphorylation catalyzed in a crystal is not significantly different than that catalyzed by a sample of protein in solution. This indicates that the protein is enzymatically active under the conditions of crystal growth. Consequently, the conformation of the enzyme obtained by X-ray crystallography under these conditions should be relevant to the catalytic mechanism of the enzyme in solution.

Because the reactions were carried out in the presence of 10 mM EDTA without added Mg^{2+} these results also indicate that the formation of the phosphoenzyme is rapid even in the absence of Mg^{2+}.

The multiple isoelectric forms obtained upon phosphorylation could be due to more than one site of phosphorylation on each monomer, various degrees of phosphorylation of an enzyme oligomer, or both. Analysis of the phosphorylated amino acid content of the protein indicated that both phosphohistidine and phosphoserine were formed in approxi-

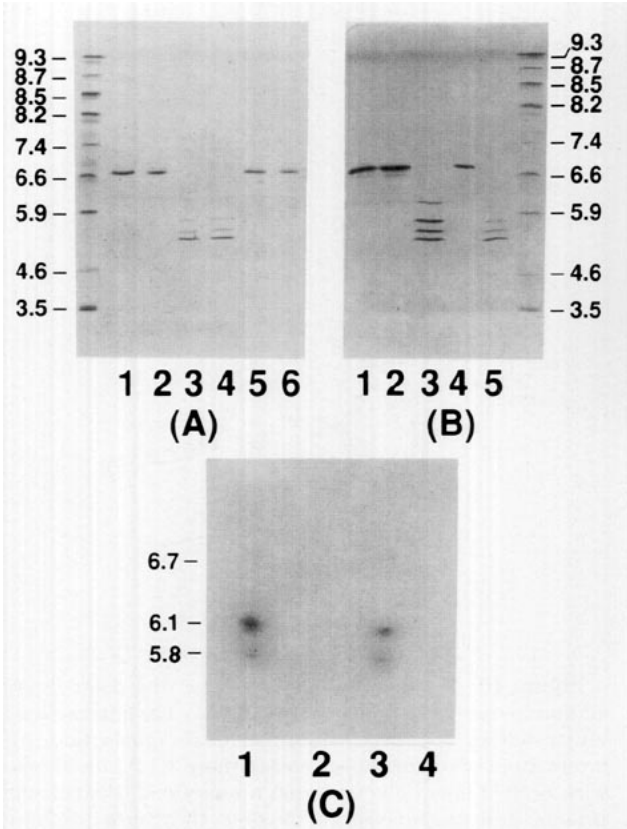

Figure 8. The form III crystals are enzymatically active as illustrated by autophosphorylation. In the presence of ATP, NDP kinase becomes phosphorylated both in solution and in crystals, as detected by a shift in pI on IEF gels. (A) Coomassie-stained IEF PAGE to assay autophosphorylation of NDP kinase in solution: lane 1, NDP kinase in a reaction mixture at pH 7·9 without nucleotide; lane 2, without nucleotide (pH 5·2); lane 3, ATP added (pH 7·9); lane 4, ATP added (pH 5·2); lane 5, ADP added (pH 7·9); lane 6, ADP added (pH 5·2). (B) Coomassie-stained IEF PAGE to assay autophosphorylation of NDP kinase in crystals: lane 1, crystals incubated with ADP (pH 5·2); lane 2, crystals incubated without nucleotide (pH 5·2); lane 3, crystals incubated with ATP (pH 5·2); lane 4, conditions identical to (A) lane 2; lane 5, conditions identical to (A) lane 4. (C) Autoradiogram of an IEF gel containing NDP kinase reacted with radiolabeled ATP. NDP kinase was incubated with: lane 1, [γ-^{32}P]ATP (pH 7·9); lane 2, [α-^{32}P]ATP (pH 7·9); lane 3, [γ-^{32}P]ATP (pH 5·2); lane 4, [α-^{32}P]ATP (pH 5·2). Only the incubation with [γ-^{32}P]ATP results in radiolabeled protein, demonstrating that the pI shift is due to phosphorylation of the enzyme.

mately equal concentrations (Muñoz-Dorado *et al.*, 1993). Our equilibrium sedimentation results indicate that the enzyme is a tetramer in solution under the conditions of the assay. The difference in the numbers of lower pI bands seen on the Coomassie-stained gels *versus* the autoradiograms is due to the concentration of the ATP. The number and the pI of isoelectric forms observed depends on the ATP concentration in the assay; at low ATP concentrations, only the partially phosphorylated forms with higher pI's are detected (not shown).

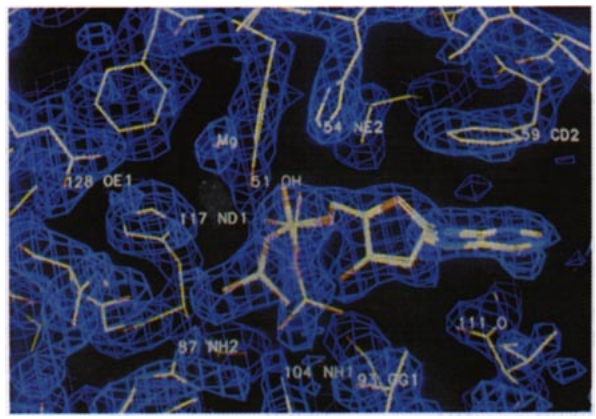

Figure 9. The refined model of the ADP·Mg^{2+}/enzyme complex. The pyrophosphate group is disordered. The two conformations modeled for the nucleotide differ principally in the position of the β-phosphate. The $2|F_{obs}|-|F_{calc}|$ electron density map (contoured at 1·2σ) is superimposed on the model. The models for both ADP conformers, B and G, are displayed together in stick representation. The model for the major ADP conformer, G, is shown with wider radius sticks.

(f) *Substrate binding*

The 2·0 Å data obtained for the co-crystal of the enzyme with ADP were easily interpretable in terms of an atomic model for the substrate. After least squares refinement against observed amplitudes using PROLSQ and the model of the native enzyme without solvent molecules, the density for the ADP was clearly discernible in the electron density map calculated with $3|F_o|-2|F_c|$ amplitudes. The model of the ADP in the enzyme/nucleotide complex is illustrated in Figure 9. The pyrophosphate moiety appears to have two distinct conformations that differ principally in the position of the β-phosphate. Both of these conformations can be accommodated with almost no changes in the ribose and only minor changes in the α-phosphate conformations. The two conformers will be denoted B and G. The occupances of the two conformers were refined by treating the atoms of the base as one group and the atoms of the sugar and pyrophosphate as a second group. As was apparent upon initial inspection of the difference electron density maps, the B conformation is less populated than the G conformation. The group occupancy of the base is 0·70 whereas the occupancies of the sugar and pyrophosphate are 0·21 and 0·54 for the B and G conformers, respectively (the scale is arbitrary and protein atoms were constrained to occupancies of 1·0). Individual temperature factors were also refined for the atoms of the nucleotide. The average isotropic temperature factors were 33·7 Å^2, 33·4 Å^2, and 31·6 Å^2 for the β-phosphate, α-phosphate and sugar of the B conformer. The temperature factors for the G conformer were slightly less; 23·3 Å^2, 27·7 Å^2, and 26·1 Å^2, for the β-phosphate, α-phosphate and sugar, respectively. The average temperature factor for the atoms of the base was 28·2 Å^2.

Table 6
Possible polar interactions between the protein and ADP

Protein atom		ADP atom	Distance (Å)
Lys11	NZ	O3*-B	2·6
		O3*-G	2·7
		O3B-G	3·0
Tyr51	OH	O3B-G	2·8
His54	NE2	O2A-B	2·4
		O1A-G	2·6
Arg87	NH2	O1B-G	3·4
Thr93	OG1	O1B-B	2·6
		PB-B	3·5
		O3B-B	3·4
Arg104	NH1	O2B-B	3·5
		O2B-G	2·8
Ile111	O	O2*-B	2·7
		O2*-G	2·7
Asn114	OD1	O3*-B	3·3
		O3*-G	3·3
Asn114	ND2	O3*-B	3·1
		O3*-G	3·0
		O2*-G	3·4
His117	ND1	O1B-G	3·1
		O3B-G	3·3
Gly118	N	O1B-G	3·4

The ADP atoms carry the suffixes B or G to distinguish the two positions occupied by the disordered group. All interactions with distances less than 3·5 Å are listed.

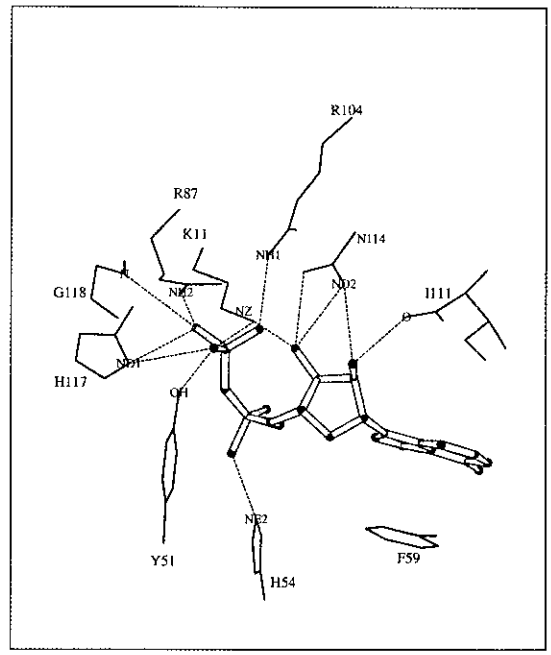

Figure 10. A schematic illustration of the polar interactions between ADP and the enzyme. The interactions illustrated are for the G conformer of the nucleotide. All interactions with distances closer than 3·5 Å are shown with broken lines. The principal interactions between the protein and the nucleotide involve the pyrophosphate moiety. The base interacts only by stacking with Phe59.

Most of the interactions with the nucleotide are with the pyrophosphate and ribose groups, while the base makes no specific interactions with the protein. The only interaction evident between the adenine ring and the protein is a stacking with Phe59. The planes of the two rings are separated by 3·6 Å. There are several polar interactions that are likely to be important for binding the substrate to the enzyme. These interactions are summarized in Table 6 and illustrated schematically in Figure 10. The ribose ring is well defined in the complex. The 3′-OH has several interactions with the protein. These include possible hydrogen bonds to side-chains of Lys11 and Asn114. The α-phosphate forms a possible salt bridge with His54. The β-phosphate forms possible salt links with Lys11, Arg87, and Arg104 in addition to hydrogen bonding with ND1 of His117, OH of Tyr51, the backbone N of Gly118 (G conformer only), and OG1 of Thr93 (B conformer only). With the exception of His54, all of the side-chains interacting with the ADP are conserved in every NDP kinase sequence that has been reported. It is possible that the positions of the α-phosphate, the β-phosphate in the B conformer, and the β-phosphate in the G conformer approximate the positions of the α, β, and γ phosphates for the substrate adenosine triphosphate. It is clear from the structure that a phosphate occupying the putative γ-phosphate site (the same site as the β-phosphate in the G conformer) would be in a good position to transfer the phosphate to the ND1 of the catalytic His117. It is not clear from the structure of the enzyme or its complex with ADP what may be the mechanism of phosphorylation of Ser119. It is unlikely that there could be direct phosphorylation of the serine by the γ-phosphate of the ATP bound to the enzyme because the distance between the hydroxyl group of Ser119 and the putative position of the γ-phosphate is 9·2 Å. However, Ser119 is much closer to the side-chain of His117 (4·6 Å and 6·2 Å between the hydroxyl group and NE2 and ND1, respectively), and its phosphorylation may be *via* the phosphohistidine intermediate.

As pointed out by Dumas *et al.* (1992), the structure of the binding site does not contain the βαβ nucleotide binding fold found in many other nucleotide-binding proteins (Rossman *et al.*, 1975), nor does the structure contain an alternative nucleotide-binding motif that has been called the palmate β-sheet fold (Yamaguchi *et al.*, 1993). In the palmate β-sheet fold, the nucleotide is found on the surface of an antiparallel β-sheet rather than at the edge as in the βαβ nucleotide binding fold, and the ATP is held in place by a glycine-rich loop. In the NDP kinase structure, the nucleotide is found at the side of the β-sheet and there is no glycine-rich loop involved in the interaction.

The surface of the enzyme has a prominent, Y-shaped cleft in it. This cleft delineates a "neck" that connects a "head" formed from residues 42 to 68 and a "torso" with residues 90 to 115 forming one "collar bone" and helix A5 forming the other. This cleft is illustrated in Figure 11. The cleft can be divided into two channels that meet in the center. These two channels are labeled B and B′ in Figure

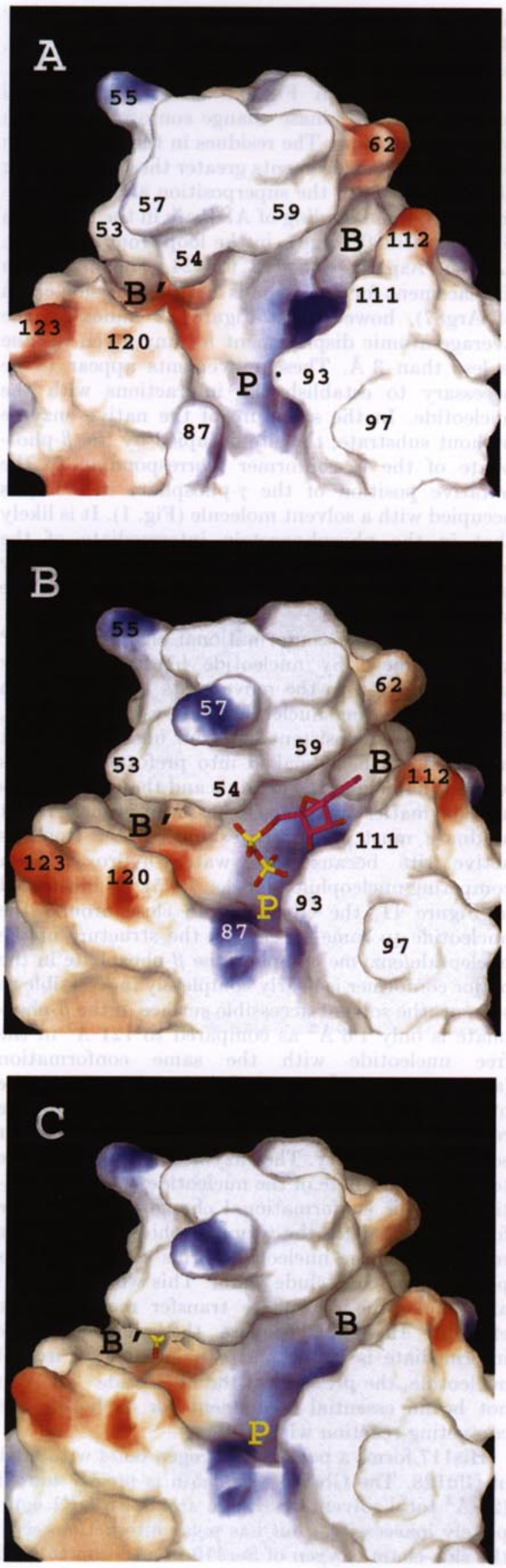

11. The B channel is somewhat wider than the B′ channel and measures about 4 to 8 Å in width and depth and about 12 Å in length. If the solution around the protein is modeled as a polarizable medium characterized with a continuum dielectric using the Poisson-Boltzmann solver of the program GRASP (Nicholls, 1992), it is possible to map the electrostatic potential onto the molecular surface of the protein. When this is done, it is apparent that the nucleotide is bound in such a fashion that the pyrophosphate moiety is contained within a deep positively-charged pocket labeled P in Figure 11. This pyrophosphate pocket is continuous with channel B that accommodates the nucleoside moiety. The concentration of positively-charged residues in the pyrophosphate-binding pocket may be an important feature in the rate-determining step of the reaction, particularly in the absence of divalent cations (see below).

It has been proposed that the allosteric domain of the regulatory subunit of aspartate transcarbamylase (ATCase, Kantrowitz & Lipscomb, 1988) may have evolved from a protein similar to NDP kinase (Kuo, 1991). The structures of both the *D. discoideum* and *M. xanthus* enzymes support this hypo-

Figure 11. A map of the electrostatic potential calculated at the molecular surface of the protein. The blue color represents regions of positive potential and the red color represents regions of negative potential. The darkest blue denotes a potential of 24 kcal mol^{-1} atomic charge $unit^{-1}$, and the darkest red denotes a potential of -24 kcal mol^{-1} atomic charge $unit^{-1}$. The molecular surface was calculated assuming a solvent sphere of 1·4 Å. The atomic radii assumed for C, O, N, and S were 1·7 Å, 1·6 Å, 1·65 Å, and 1·9 Å, respectively. The atomic charges are zero for all atoms except LysNZ (+1·0), ArgNH1 and NH2 (+0·5), AspOD1 and OD2 (−0·5), and GluOE1 and OE2 (−0·5). The external dielectric constant was assumed to be 80. The internal dielectric constant was assumed to be 2·0. The ionic strength of the solvent was assumed to be zero. The solvation reaction potential calculations were done using the Poisson-Boltzmann solver of the program GRASP (Nicholls, 1992). The molecular surface was also calculated and displayed by GRASP. A. The surface potential for the enzyme in the absence of nucleotide. B. The surface potential of NDP kinase in the ADP/enzyme complex. The nucleotide is superimposed on the surface but was not used in either the potential calculation or the molecular surface calculation. The walls of the channel labeled B change conformation slightly, conforming more tightly to the nucleotide and decreasing the solvent-accessible surface area of the nucleotide, particularly the terminal phosphate. C. The ATP from the complex with the allosteric domain of the regulatory subunit of ATCase (Protein Data Bank entry 4at1) is superimposed on the potential surface of NDP kinase from B using the rigid body transformation that optimally superimposes the β-sheets of these two proteins. The phosphate visible in the B′ channel is the α-phosphate of the ATP bound to ATCase. The remainder of the superimposed nucleotide is buried beneath the surface in a sterically disallowed fashion. The nucleotide binding is clearly different than that proposed on the basis of the structure of NDP kinase from *D. discoideum* (Dumas *et al.*, 1992).

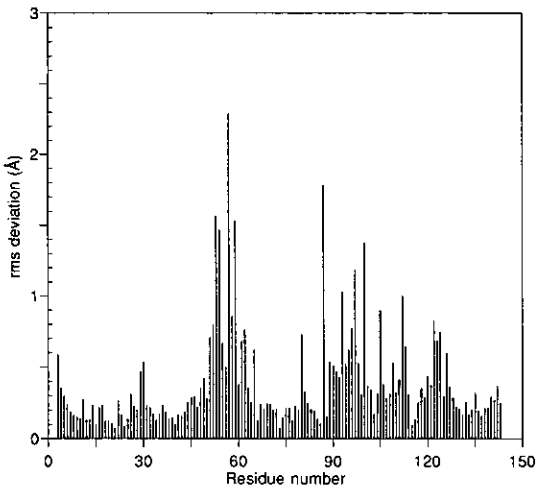

Figure 12. Average rms deviations between atoms of the native enzyme and the atoms of the enzyme in the complex with ADP *versus* residue number. All atoms were used for the superimposition and for the rms calculation. These correspond largely to movements of side chains that form the interactions with the nucleotide.

thesis in that the overall fold is very similar. However, although the similarity in the overall folds of the two proteins is striking, the interaction of NDP kinase with the nucleotide is clearly distinct from that of ATCase. The most distinctive difference between the nucleotide binding for the two proteins is that in ATCase the nucleotide is located on the surface of the antiparallel β-sheet whereas in *M. xanthus* NDP kinase the nucleotide is at the side of the sheet. The presence of helices partially covering the surface of the NDP kinase β-sheet precludes the mode of binding reported for ATCase. The second channel (labeled B′ in Fig. 11) on the surface of NDP kinase also terminates in the pyrophosphate-binding pocket. This channel is formed between the loop from 46 to 54 and helix A5. Although this channel appears to be approximately the right size to accommodate the nucleoside moiety, there is no density in the map consistent with such alternative binding. Using the rigid-body transformation that optimally superimposes the allosteric domain of the regulatory subunit of ATCase on the β-sheet of NDP kinase, it is possible to position the nucleotide of the ATCase structure (Stevens *et al.*, 1990) onto NDP kinase. This places the nucleotide roughly over the center of the β-sheet in such a manner that its α-phosphate protrudes into the B′ channel and the remainder of the nucleotide is occluded by the C-terminal helix of NDP kinase and the loop from 46 to 54, as illustrated in Figure 11C. Based on the structure of an enzymatically inactive mutant, Dumas *et al.* (1992) proposed that the nucleotide binding for NDP kinase and ATCase would be similar and that the nucleotide would occupy channel B′. Preliminary crystallographic analyses of complexes of NDP kinase with non-hydrolyzable nucleoside triphosphate analogs and with ATP indicate that the nucleoside triphosphates also occupy the B channel rather than the B′ channel (Perisic, O., Webb, P. A. & Williams, R. L., unpublished results).

As illustrated in Figures 11 and 12, several residues in NDP kinase change conformation upon nucleotide binding. The residues in the protein with average rms displacements greater than 0·7 Å (using all atoms for both the superposition and rms determination) upon binding of ADP are in the loop from 51 to 62, Glu80, Arg87, in the loop from 93 to 100, Lys105, Asp112, and 122 to 124. The maximum displacement for any atom is 7 Å (for the side chain of Arg87), however, as Figure 12 indicates, the average atomic displacement for any given residue is less than 3 Å. These movements appear to be necessary to establish the interactions with the nucleotide. In the structure of the native enzyme without substrate, the site occupied by the β-phosphate of the G conformer (corresponding to the putative position of the γ-phosphate in ATP) is occupied with a solvent molecule (Fig. 1). It is likely that in the phosphoprotein intermediate of the enzymatic mechanism, the phosphate covalently bound to ND1 of His117 is also occupying the same site.

In general, the conformational changes in NDP kinase induced by nucleotide binding are fairly small compared to the movements that have been reported for other nucleotide kinases (Schulz *et al.*, 1990). This is consistent with our observation that nucleotides can be soaked into preformed crystals without damaging the crystals and that the crystals are enzymatically active. It has been proposed that a kinase must efficiently exclude water from its active site because the water hydroxyl is a competing nucleophile (Jencks, 1975). As illustrated in Figure 11, the enzyme does close around the nucleotide to some extent. In the structure of the nucleotide/enzyme complex, the β-phosphate in the major conformer is nearly completely inaccessible to solvent; the solvent-accessible surface of the β-phosphate is only 1·6 Å^2 as compared to 121 Å^2 in the free nucleotide with the same conformation (assuming a 1·9 Å radius for phosphorus and the other atomic radii as given in Fig. 11). However, the remainder of the nucleotide retains a much greater solvent accessibility. The enzyme is able to bury the terminal phosphate of the nucleotide with only relatively minor conformational changes. The enzyme forms a pocket for the terminal phosphate and the remainder of the nucleotide forms a "lid" for this pocket so as to exclude water. This would presumably make the phosphate transfer reaction more efficient. However, because the phosphoenzyme intermediate is stable and can be isolated free of nucleotide, the presence of the nucleotide "lid" can not be an essential component for excluding the competing reaction with water.

His117 forms a possible hydrogen bond with OE1 of Glu128. The Glu128 side-chain is mostly buried (20 Å^2 total solvent-accessible area with OE1 completely inaccessible) but has polar interactions with the side-chain oxygen of Ser119 in addition to NE2

of His117 (Fig. 1). The interaction of Glu128 with His117 may increase the nucleophilicity of His117 in a manner reminiscent of the interaction present between Asp and His in the catalytic triad of the serine proteases and lipases (Brady *et al.*, 1990). However, because of the negative charge of the phosphate in the phosphohistidine intermediate, the role of the Glu128 is probably not as critical as that of the catalytic aspartate in the serine proteases.

By collecting diffraction data from co-crystals in the presence and in the absence of Mg^{2+}, we were able to define the site of the metal in the complex using difference Fourier analyses. The Mg^{2+} site is near the Mn^{2+} position determined using anomalous scattering for the structure of the enzyme complexed with Mn^{2+}·ADP (Perisic, O., Webb, P. A. & Williams, R. L., unpublished results). The association of the Mg^{2+} with the nucleotide is much closer than with the protein. The Mg^{2+} is 2·9 Å from the nearest oxygen of the α-phosphate of the ADP (G conformer). The positions of the sugar and base moiety do not differ in complexes with or without Mg^{2+}. There are, however, shifts in the positions of the phosphates. The association of the Mg^{2+} with the α-phosphate is consistent with the dissociative mechanism that was proposed for sulfuryl and phosphoryl transfer to the enzyme (Peliska & O'Leary, 1991) in which the metal ion chelates the ADP leaving group, i.e. coordinates the α- and β-phosphates of $ADPSO_3$ or ATP. The protein residue nearest Mg^{2+} is Asp120 in the vicinity of the junction of the B′ channel with the pyrophosphate pocket. Although the overall transfer of a phosphoryl group from one nucleotide to another requires Mg^{2+}, no divalent cation is required for the autophosphorylation activity of the enzyme. The metal independent autophosphorylation is consistent with our observation that there is little change in the conformation of the ADP·enzyme complex in the presence or absence of Mg^{2+}. The work of Peliska and O'Leary indicates that the less negatively charged sulfuryl group of the sulfoenzyme intermediate can be transferred readily to a nucleoside diphosphate acceptor without a divalent cation. This may imply that electrostatic effects can determine the rate of transfer from the covalent enzyme intermediate to the acceptor (Peliska & O'Leary, 1991).

(g) *The Kpn loop*

The region from 93 to 112 (*M. xanthus* numbering) constitutes what has been referred to as the Kpn loop (Dumas *et al.*, 1992). In *M. xanthus*, this region includes helix A4. Although a proline to serine mutation in the *D. melanogaster* NDP kinase Awd at the position homologous to *M. xanthus* Pro95 has profound consequences *in vivo*, this mutation does not affect the catalytic efficiency (k_{cat}/K_m) of the enzyme (Lascu *et al.*, 1992). Consequently, it was proposed that this loop may interact with other cellular proteins (Lascu *et al.*, 1992). In *D. discoideum* NDP kinase, the loop is found at the center of the hexamer (Dumas *et al.*, 1992) and appears to be important for oligomerization of the enzyme. In *M. xanthus* NDP kinase, the loop is at the outer extremities of the tetramer, as illustrated in Figure 13. The loop is clearly not involved in intermolecular contacts within the tetramer, however, its conformation could be important for the interaction of the enzyme with ADP. As indicated in Table 6, Thr93 has a possible hydrogen bond with an oxygen of the β-phosphate. Residues of the Kpn loop in *M. xanthus* NDP kinase undergo displacements upon binding substrates that are among the largest found in the enzyme (Fig. 12). It is not known whether the corresponding proline to serine mutation in *M. xanthus* NDP kinase has any effect on the enzymatic activity.

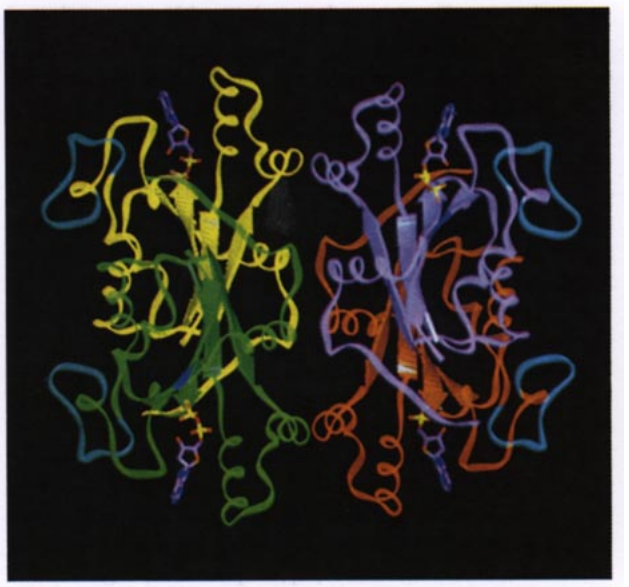

Figure 13. A view of the tetrameric enzyme/ADP complex illustrating that both the active sites and Kpn loops (light blue) of the monomers are directed toward the outer extremities of the tetramer. This differs from the conformation of NDP kinase from *D. discoideum* where the Kpn loops are located at the center of a hexamer.

(h) *Consensus nucleotide binding sequence motif*

M. xanthus NDP kinase has two sequence motifs that are similar to motifs found in other GTP-binding proteins such as *H-ras* (McCormick *et al.*, 1985). It was suggested that these sequences were important for nucleotide binding in *M. xanthus* NDP kinase (Muñoz-Dorado *et al.*, 1993). These motifs are GXXGK (residues 18 to 22) and DXXG (residues 88 to 91). In contrast to GTP-specific proteins, however, NDP kinase does not contain the consensus sequence reported to be important for guanine recognition (McCormick *et al.*, 1985; Muñoz-Dorado *et al.*, 1990*a*; Wallet *et al.*, 1990). Studies of mutants of *M. xanthus* NDP kinase indicated that mutations of the glycine residues in these conserved motifs abolished activity of the enzyme (mutations G21V or G91V), whereas

mutations affecting charged residues produced phenotypes with activities identical to the wild-type enzyme (mutations K22N or D88G) (Muñoz-Dorado *et al.*, 1993). Although the GXXGK motif appears to be analogous with a phosphoryl-binding motif, with mutation of glycine yielding inactive enzymes, our structural studies suggest that the GVIGK sequence in *M. xanthus* NDP kinase is not near the phosphate binding site and that the loss of activity may be due to disrupting interactions between members of an obligate dimer because this sequence occurs near the beginning of helical segment A1 at the dimer interface. This role of Gly21 as opposed to a part of a pyrophosphate binding loop is also consistent with the NDP kinase sequences that have been recently reported. Gly21 is conserved whereas Gly18 and Lys22 are not. The loss of activity of the G91V mutant is probably due to disruption of conformation in the portion of the loop involved in interaction with the β-phosphate (Arg87 and Thr93).

We are grateful to Olga Perisic for protein purification, mutagenesis, crystallization, and for reading the manuscript and to Jo Butler for the equilibrium sedimentation analysis. We thank Ray Nanni and Kim Henrick for helpful discussions and assistance with synchrotron X-ray data collection. The work was supported by a grant from American Cancer Society (BE-139) to R.L.W. and by the Medical Research Council, the Department of Trade and Industry, and ICI under the Protein Engineering LINK programme (R.L.W.). E.A. thanks the Center for Advanced Biotechnology and Medicine, the New Jersey Commission on Science and Technology, and NIH grant (AI27690) for support. The work of J.M.D., M.I. and S.I. was supported by NIH grant (GM26843) to S.I. D.A.O. was supported by a Rutgers-UMDNJ Biotechnology Training Program (GM08339) from NIH. We thank the Science and Engineering Research Council for access to the synchrotron radiation facilities at Daresbury Laboratory. We thank Richard Leidich for technical assistance and Robert Sweet, Alfredo Jacobo-Molina and Xiaode Lu for help with preliminary synchrotron data collection at BNL. The X-ray amplitudes, phases, and derived atomic coordinates for the structures described here have been deposited into the Brookhaven Protein Data Bank (Entry 1NCK).

References

Biggs, J., Hersperger, E., Steeg, P. S., Liotta, L. A. & Shearn, A. (1990). A Drosophila gene that is homologous to a mammalian gene associated with tumor metastasis codes for a nucleoside diphosphate kinase. *Cell*, **63**, 933–940.

Blundell, T. L. & Johnson, L. N. (1976). *Protein Crystallography*, Academic Press, Inc., London.

Brady, L., Brzozowski, A. M., Derewenda, Z. S., Dodson, E., Dodson, G., Tolley, S., Turkenburg, J. P., Christiansen, L., Huge-Jensen, B., Norskov, L., Thim, L. & Menge, U. (1990). A serine protease triad forms the catalytic centre of a triacylglycerol lipase. *Nature (London)*, **343**, 767–770.

Brunger, A. (1992). XPLOR. Yale University, New Haven, CT.

Dodson, E. J. (1992). Molecular replacement. In *CCP4 Study Weekend*, SERC (U.K.) (Dodson, E. J., Grover S. & Woolf, W., eds), pp. 84–86, Daresbury Laboratory, Warrington, U.K.

Dumas, C., Lebras, G., Wallet, V., Lacombe, M.-L., Veron, M. & Janin, J. (1991). Crystallization and preliminary X-ray diffraction studies of nucleoside diphosphate kinase from *Dictyostelium discoideum*. *J. Mol. Biol.* **217**, 239–240.

Dumas, C., Lascu, I., Morera, S., Glaser, P., Fourme, R., Wallet, V., Lacombe, M.-L., Veron, M. & Janin, J. (1992). X-ray structure of nucleoside diphosphate kinase. *EMBO J.* **11**, 3203–3208.

Evans, P. (1992). IPMADNES. Cambridge, U.K.

Francis, B., Overmeyer, J., John, W., Marshall, E. & Haley, B. (1989). Prevalence of nucleoside diphosphate kinase autophosphorylation in human colon carcinoma versus normal colon homogenates. *Mol. Carcinogen.* **2**, 168–178.

Furey, W. (1992). PHASES. Pittsburgh, PA.

Ginther, C. L. & Ingraham, J. L. (1974). Nucleoside diphosphate kinase of *Salmonella typhimurium*. *J. Biol. Chem.* **249**, 3406–3411.

Hama, H., Almaula, N., Lerner, C. G., Inouye, S. & Inouye, M. (1991). Nucleoside diphosphate kinase from *Escherichia coli*; its overproduction and sequence comparison with eukaryotic enzymes. *Gene*, **105**, 31–36.

Hemmerich, S. & Pecht, I. (1992). Oligomeric structure and autophosphorylation of nucleoside diphosphate kinase from rat mucosal mast cells. *Biochemistry*, **31**, 4580–4587.

Hendrickson, W. A. & Konnert, J. H. (1980). Incorporation of stereochemical information into crystallographic refinement. In *Computing in Crystallography* (Diamond, R., Ramaseshan, S. & Venkatesan, K., eds), pp. 13.01–13.25, Indian Academy of Sciences, Bangalore.

Jencks, W. P. (1975). Binding energy, specificity, and enzymic catalysis: the circe effect. *Advan. Enzymol.* **43**, 219–410.

Jones, T. A., Zou, J.-Y., Cowan, S. W. & Kjeldgaard, M. (1991). Improved methods for building protein models in electron density maps and the location of errors in these models. *Acta. Crustallogr. sect. A*, **47**, 110–119.

Jong, A. Y. & Ma, J. J. (1991). *Saccharomyces cerevisae* nucleoside diphosphate kinase: purification, characterization, and substrate specificity. *Arch. Biochem. Biophys.* **291**, 241–246.

Kabsch, W. (1978). A solution for the best rotation to relate two sets of vectors. *Acta Crystallogr. sect. A*, **32**, 922–923.

Kantrowitz, E. R. & Lipscomb, W. N. (1988). *Escherichia coli* aspartate transcarbamylase. The relation between structure and function. *Science*, **241**, 669–674.

Karlsson, A., Reichard, P. & Eckstein, F. (1990). The metabolism of 3′-azido-2′,3′-dideoxyguanosine in CEM cells. *Biochem. Biophys. Res. Commun.* **166**, 273–279.

Kikkawa, S., Takahashi, K., Takahashi, K., Shimada, N., Ui, M., Kimura, N. & Katada, T. (1990). Conversion of GDP into GTP by nucleoside diphosphate kinase on the GTP-binding proteins. *J. Biol. Chem.* **265**, 21536–21540.

Kraulis, P. J. (1991). MOLSCRIPT: a program to produce both detailed and schematic plots of protein structures. *J. Appl. Crystallogr.* **24**, 946–950.

Kuo, L. C. (1991). Generation of allosteric enzymes from nonallosteric forms. *Methods Enzymol.* **202**, 706–727.

Lamzin, V. S. & Wilson, K. S. (1993). Automated refinement of protein models. *Acta. Crystallogr. sect. D*, **49**, 129–147.

Lascu, I., Chaffotte, A., Limbourg-Bouchon, B. & Veron, M. (1992). A pro/ser substitution in nucleoside diphosphate kinase of *Drosophila melanogaster* (mutation *killer of prune*) affects stability but not catalytic efficiency of the enzyme. *J. Biol. Chem.* 267, 12775-12781.

Lee, B. & Richards, F. M. (1971). The interpretation of protein structures: estimation of static accessibility. *J. Mol. Biol.* **55**, 379–400.

Leone, A., Flatow, U., King, C. R., Sandeen, M. A., Margulies, I. M. K., Liotta, L. A. & Steeg, P. S. (1991). Reduced tumor incidence, metastatic potential and cytokine responsiveness of *nm23*-transfected melanoma cells. *Cell*, **65**, 25–35.

Liotta, L. A. & Steeg, P. S. (1990). Clues to the function of Nm23 and Awd proteins in development, signal transduction, and tumor metastasis provided by studies of *Dictyostelium discoideum*. *J. Nat. Cancer Inst.* **82**, 1170–1172.

McCormick, F., Clark, B. F. C., la Cour, T. F. M., Kjeldgaard, M., Norskov-Lauritsen, L. & Nyborg, J. (1985). A model for the tertiary structure of p21, the product of the *ras* oncogene. *Science*, **230**, 78–82.

McPherson, A. (1982). *Preparation and Analysis of Protein Crystals*. J. Wiley & Sons, New York.

Mourad, N. & Parks, R. E., Jr (1966). Erythrocytic nucleoside diphosphokinase. II. Isolation and kinetics. *J. Biol. Chem.* **241**, 271 278.

Muñoz-Dorado, J., Inouye, M. & Inouye, S. (1990*a*). Nucleoside diphosphate kinase from *Myxococcus xanthus*. I. Cloning and sequencing of the gene. *J. Biol. Chem.* **265**, 2702 2706.

Muñoz-Dorado, J., Inouye, S. & Inouye, M. (1990*b*). Nucleoside diphosphate kinase from *Myxococcus xanthus*. II. Biochemical characterization. *J. Biol. Chem.* **265**, 2707–2712.

Muñoz-Dorado, J., Almaula, N., Inouye, S. & Inouye, M. (1993). Autophosphorylation of nucleoside diphosphate kinase from *Myxococcus xanthus*. *J. Bacteriol.* **175**, 1176 1181.

Nagai, K., Oubridge, C., Jessen, T. H., Li, J. & Evans, P. R. (1990). Crystal structure of the RNA-binding domain of the U1 small nuclear ribonucleoprotein A. *Nature (London)*, **348**, 515–520.

Nicholls, A. (1992). GRASP: Graphical Representation and Analysis of Surface Properties. New York.

Nickerson, J. A. & Wells, W. W. (1984). The microtubule-associated nucleoside diphosphate kinase. *J. Biol. Chem.* **259**, 11297–11304.

Ohtsuki, K., Yokoyama, M., Ikeuchi, T., Ishida, N., Sugita, K. & Satoh, K. (1986). Rapid induction of nucleoside diphosphate kinase in HeLa S3 cells by human-type interferons. *FEBS Letters*, **196**, 145–150.

Parks, R. E., Jr & Agarwal, R. P. (1973). Nucleoside diphosphokinases. In *The Enzymes* (Boyer, P. D., ed.), vol. 8, pp. 307–334, Academic Press, New York.

Peliska, J. A. & O'Leary, M. H. (1991). Sulfuryl transfer catalyzed by phosphokinases. *Biochemistry*, **30**, 1049–1057.

Pflugrath, J. W. (1989). MADNES. Cold Spring Harbor, NY.

Ramakrishnan, C. & Ramachandran, G. N. (1965). Stereochemical criteria for polypeptide and protein chain conformations. *Biophys. J.* **5**, 909–933.

Randazzo, P. A., Northup, J. K. & Kahn, R. A. (1992). Regulatory GTP-binding proteins (ADP-ribosylation factor, G(t), and RAS) are not activated directly by nucleoside diphosphate kinase. *J. Biol. Chem.* **267**, 18182 18189.

Richardson, J. S. (1981). The anatomy and taxonomy of protein structure. *Advan. Protein Chem.* **34**, 167–363.

Rossmann, M. G., Liljas, A., Branden, C.-I. & Banaszak, L. J. (1975). Evolutionary and structural relationships among dehydrogenases. In *The Enzymes* (Boyer, P. D., ed.), vol. 11, pp. 61–102, Academic Press, New York.

Rould, M. A., Perona, J. J., Soll, D. & Steitz, T. A. (1989). Structure of *E. coli* glutaminyl-tRNA synthetase complexed with $tRNA^{Gln}$ and ATP at 2 Å resolution. *Science*, **246**, 1135–1142.

Schulz, G. E., Muller, C. W. & Diederichs, K. (1990). Induced-fit movements in adenylate kinases. *J. Mol. Biol.* **213**, 627–630.

Stevens, R. C., Gouaux, J. E. & Lipscomb, W. N. (1990). Structural consequences of effector binding to the T state of aspartate carbamoyltransferase: crystal structures of the unligated and ATP- and CTP-complexed enzymes at 2·6 Å resolution. *Biochemistry*, **29**, 7691–7701.

Teng, D. H. F., Engele, C. M. & Venkatesh, T. R. (1991). A product of the *prune* locus of *Drosophila* is similar to mammalian GTPase-activating protein. *Nature (London)*, **353**, 437–440.

Wallet, V., Mutzel, R., Troll, H., Barzu, O., Wurster, B., Veron, M. & Lacombe, M.-L. (1990). *Dictyostelium* nucleoside diphosphate kinase highly homologous to Nm23 and Awd proteins involved in mammalian tumor metastasis and *Drosophila* development. *J. Nat. Cancer Inst.* **82**, 1199–1202.

Wieland, T. & Jakobs, K. H. (1989). Receptor-regulated formation of GTP[γS] with subsequent persistent G_s-protein activation in membranes of human platelets. *FEBS Letters*, **245**, 189–193.

Williams, R. L., Muñoz-Dorado, J., Jacobo-Molina, A., Inouye, S., Inouye, M. & Arnold, E. (1991). Crystallization and preliminary X-ray diffraction analysis of nucleoside diphosphate kinase from *Myxococcus xanthus*. *J. Mol. Biol.* **220**, 5–7.

Woods, D. F. & Bryant, P. J. (1991). The Discs-large tumor suppressor gene of *Drosophila* expresses a guanylate kinase homolog localized at septate junctions. *Cell*, **65**, 451–464.

Yamaguchi, H., Kato, H., Hata, Y., Nishioka, T., Kimura, A., Oda, J. & Katsube, Y. (1993). Three-dimensional structure of the glutathione synthetase from *Escherichia coli* B at 2·0 Å resolution. *J. Mol. Biol.* **229**, 1083–1100.

Edited by B. W. Matthews

Note added in proof: The X-ray structure of *D. discoideum* NDP kinase in a complex with ADP has recently been solved (S. Moréra, I. Lascu, C. Dumas, G. LeBras, P. Briozzo, M. Véron, J. Janin, *Biochemistry*, in the press). Prof. J. Janin has kindly made the coordinates for this structure available to us. The dimeric interaction and nucleotide binding are strikingly similar to what we have observed for the *M. xanthus* NDP kinase despite the difference in quaternary structure (hexamer *versus* tetramer) and relatively low sequence homology.